INORGANIC CHEMISTRY FRONTIERS

CCS 中国化学会 CHINESE CHEMICAL SOCIETY

ROYAL SOCIETY OF CHEMISTRY

Antimony Doping to Enhance Luminescence of Tin (IV)-Based Hybrid Metal Halides

Journal:	*Inorganic Chemistry Frontiers*
Manuscript ID	QI-RES-04-2022-000884.R1
Article Type:	Research Article
Date Submitted by the Author:	13-Jun-2022
Complete List of Authors:	Liu, Kunjie; University of Science and Technology Beijing Hao, Shiqiang; Northwestern University, Materials Science Cao, Jindong; University of Science and Technology Beijing Lin, Jiawei; University of Science and Technology Beijing, Fan, Liubing; University of Science and Technology Beijing zhang, Xusheng ; University of Science and Technology Beijing Guo, Zhongnan; University of Science and Technology Beijing, Department of Chemistry, School of Chemistry and Biological Engineering Wolverton, Chris; Northwestern University, Department of Materials Science and Engineering Zhao, Jing; University of Science and Technology Beijing, School of Materials Science and Engineering Liu, Quanlin; University of Science and Technology Beijing, School of Materials science & engineering

Antimony Doping to Enhance Luminescence of Tin (IV)-Based Hybrid Metal Halides

Kunjie Liu,[a] Shiqiang Hao,[b] Jindong Cao,[a] Jiawei Lin,[c] Liubing Fan,[a] Xusheng Zhang,[a] Zhongnan Guo,[c] Christopher Wolverton,[b] Jing Zhao,[*a] and Quanlin Liu,[a]

[a]The Beijing Municipal Key Laboratory of New Energy Materials and Technologies, School of Materials Sciences and Engineering, University of Science and Technology Beijing, Beijing 100083, P. R. China.

[b]Department of Materials Science and Engineering, Northwestern University, Evanston, Illinois 60208, United States.

[c]Department of Chemistry, School of Chemistry and Biological Engineering, University of Science and Technology Beijing, Beijing, 100083, P. R. China.

ABSTRACT:

Lead-based organic–inorganic metal halides (OIMHs) have recently attracted special attention due to their efficient broadband photoluminescence. However, the toxicity of lead poses a challenge for their further development. Here, we selected Sn (IV) as the metal center to synthesize the environmentally friendly and stable luminescent OIMHs $(C_9H_{15}N_3)_2SnCl_8$ and $(C_9H_{15}N_3)_2SnBr_8$ ($C_9H_{13}N_3$ is 1-(2-pyridyl)piperazine). Both compounds possess zero-dimensional structures, crystallizing in the monoclinic space group $P2_1/c$, and their optical band gaps were experimentally determined to be 3.19 and 2.60 eV, respectively. Under UV excitation at room temperature, $(C_9H_{15}N_3)_2SnCl_8$ exhibited double-peak emissions centered at 405 and 688 nm, which were attributed to the organic cation and inorganic octahedra, respectively. Upon introducing $5s^2$-lone-pair-containing Sb^{3+} in $(C_9H_{15}N_3)_2SnCl_8$, self-trapped emission was promoted, and the photoluminescence quantum yield increased from ~1% to ~17.84%. This work suggests effective strategies for finding environmentally friendly stable OIMHs and for further enhancing the luminescence properties through lone-pair-containing cation doping.

Introduction

Organic–inorganic metal halides (OIMHs), as a new type of material, can be used in many fields owing to their diverse structure and semiconducting properties, including in photoluminescence (PL) applications, light-emitting diodes (LEDs), sensors, and lasers.[1-3] Recently, low-dimensional OIMHs have been shown to exhibit excellent PL with efficient broadband emission covering the entire visible-light range; in addition, they have the potential to achieve single-component white-light emission.[4-7] Low-dimensional lead-based OIMHs have displayed very broad PL;[8-10] however, the toxicity of lead hinders their commercialization.[11] To synthesize less toxic OIMHs, the isovalent element Sn(II) is a good substitute for Pb^{2+}, and the resulting materials generally exhibit very efficient PL; however, Sn(II) can be easily oxidized to Sn(IV), indicating poor ambient stability.[12-14] Thus, using Sn^{4+} to replace Pb^{2+} has become a feasible method.[15-17]

Zero-dimensional (0D) OIMHs, with isolated PL centers separated by organic cations and self-trapped exciton (STE) emission, are emerging as a new class of rare-earth-metal-free solid-state phosphors.[18] Sn(IV)-based OIMHs exhibit excellent stability and are characterized by a Sn six-coordinate octahedron with excellent PL properties;[19] but, there are limited reports on Sn(IV)-based OIMHs. Quasi-white light emission was achieved using $(C_{12}H_{14}N_2O_2S)[SnCl_6]\cdot H_2O$; the shoulder emission peak at 482 nm originated from the contribution of $(C_{12}H_{14}N_2O_2S)^{2+}$ cations, and the strong emission peak at 592 nm was attributed to the $[SnCl_6]^{2-}$ octahedra.[20] Recently, Lin's group synthesized a new 0D OIMH $(C_5N_2H_{14})SnCl_6$ that exhibited white-light emission, where the high-energy emission peak (570 nm) was attributed to the $(C_5N_2H_{14})^{2+}$ organic ion and the low-energy emission peak (680 nm)

was attributed to the $[SnCl_6]^{2-}$ octahedra.[21, 22] Nevertheless, given the nearly standard octahedral configuration and the absence of ns^2 electrons, the emission intensity of Sn(IV)-based OIMHs is relatively weak compared to that of lone-pair-containing Sn^{2+}-based compounds,[4, 23] and hence enhancing their luminescence performance is a concern.[24]

The $5s^2$-electron-containing six coordinated Sb^{3+} has a cation radii of 0.76 Å, which is comparable to that of Sn^{4+} (0.69 Å). From the structure point of view, Sb^{3+} can share the same site with Sn^{4+}; therefore, it can be used as a doping ion to enhance the optical properties of OIMHs.[25, 26] The combination of luminescent organic cations and an inorganic luminescent center can broaden the light-emitting wavelength range and facilitate the realization of single-component white-light emission. In this study, an organic species with blue emission, $C_9H_{13}N_3$ (1-(2-pyridyl)piperazine), was used as an organic cation in an attempt to synthesize Sn(IV) hybrid halides with the aim of achieving broadband emission. Because the Sb^{3+} ion has the advantages of being non-toxic and stable and exhibiting efficient broadband ns^2 emission, it was used as a dopant to improve the PL of the obtained compounds.[27, 28]

Using the above ideas, $(C_9H_{15}N_3)_2SnCl_8$ and $(C_9H_{15}N_3)_2SnBr_8$ were synthesized, both of which have 0D structures with Sn-based octahedra and halide anions separated by organic cations. Optical characterization revealed that both compounds exhibited very low PL at room temperature. Sb^{3+} doping was conducted to improve the PL properties of $(C_9H_{15}N_3)_2SnCl_8$, and the luminescent mechanism is discussed in detail. $(C_9H_{15}N_3)_2(Sn_{0.77}Sb_{0.23})Cl_8$ exhibited the highest PL intensity. Our work highlights several environmentally friendly luminescent materials and suggests an efficient lone-pair-containing cation-doping route to enhance the luminescent performance.

Experimental Section

Materials

$C_9H_{13}N_3$ (1-(2-pyridyl) piperazine) with a purity of 97% was obtained from HWRK CHEM. $SnCl_2$ (99.9%), $SnBr_2$ (99.9%), and $SbCl_3$ (99.9%) were purchased from Aladdin Company. HCl (36–38 wt.% in H_2O), N,N-dimethylformamide (DMF; Analytical Reagent, AR), and HBr (48 wt.% in H_2O) were obtained from Beijing Chemical Works.

Synthesis

$C_9H_{13}N_3$ (260 μL) and SnX_2 ($SnCl_2$: 0.189 g, $SnBr_2$: 0.278 g) were dissolved in 2-mL HX (X = Cl, Br) and 1-mL DMF solution and heated at ~90 °C with continuous stirring until the solution became clear. The mixed solution was stored in a 90 °C oven for 12 h and then slowly cooled (0.5 °C/h) to room temperature. Finally, high-quality transparent crystals were obtained. The reaction yield based on Sn element was ~76% and ~65% for $(C_9H_{15}N_3)_2SnCl_8$ and $(C_9H_{15}N_3)_2SnBr_8$, respectively. Sb-doped $(C_9H_{15}N_3)_2SnCl_8$ was synthesized using the same method with feeding molar ratios of $SbCl_3/(SnCl_2+SbCl_3)$ of 0.09, 0.17, 0.23, 0.28, 0.33, and 0.37.

Characterization

Powder X-ray diffraction (PXRD) measurements were performed on a PANalytical Empyrean diffractometer operating at 45 kV and 40 mA with Cu Kα radiation. A Rigaku XtaLAB PRO single-crystal diffractometer with Mo Kα radiation was used for single-crystal X-ray diffraction, and the SHELXTL software package was used for refinement.[29] A JEOL JSM-6510A scanning electron microscope was used for scanning electron microscopy (SEM)

and energy-dispersive X-ray spectroscopy (EDS) analyses. Thermogravimetric analysis (TGA) was performed using a Setaram Labsys Evo instrument with a heating rate of 10 °C/min. A Hitachi UH4150 was used to collect diffuse reflectance spectra. Agilent 725ES and Agilent 5110 instruments were used for inductively coupled plasma optical emission spectrometry (ICP-OES). X-ray photoelectron spectroscopy (XPS) was performed using a monochromatic Al Kα X-ray source (hv = 1486.6 eV) with a power of 150 W (Axis Ultra, Kratos Corporation of Shimadzu Group). The binding energies were referred to the O-1s binding energy at 529 eV. A FLS920 (Edinburgh Instruments Ltd., UK) with a 150-W Xenon lamp was used to obtain the steady-state PL spectra, photoluminescence quantum yield (PLQY), temperature-dependent spectra, and luminescence attenuation curve.

Calculation

Periodic boundary conditions and a plane-wave basis set implemented in the Vienna ab initio simulation package were used for the Density functional theory (DFT) calculations.[30] Using a basis set energy cutoff of 500 eV, the DFT calculation converged to ~3 meV/cation, and the dense k grid in the Brillouin zone corresponds to 4000 k-points for each reciprocal atom.

Results and discussion

The crystals of $(C_9H_{15}N_3)_2SnCl_8$ and $(C_9H_{15}N_3)_2SnBr_8$ were synthesized by mixing the organic substance ($C_9H_{13}N_3$) with DMF, adding SnX_2 (X = Cl, Br), and dissolving the mixture in HCl (HBr) and cooling slowly to room temperature. Both $(C_9H_{15}N_3)_2SnCl_8$ and $(C_9H_{15}N_3)_2SnBr_8$ exhibited very good crystal quality, and the crystal size was large (~ 1 cm), as shown in **Figure 1**. EDS analysis indicated a metal/halide ratio of ~1:8.11 for

$C_9H_{15}N_3)_2SnCl_8$ and ~1:7.82 for $(C_9H_{15}N_3)_2SnBr_8$, and SEM elemental mapping of $(C_9H_{15}N_3)_2SnCl_8$ and $(C_9H_{15}N_3)_2SnBr_8$ revealed the homogeneous distribution of the constituent elements **(Figure S1)**.

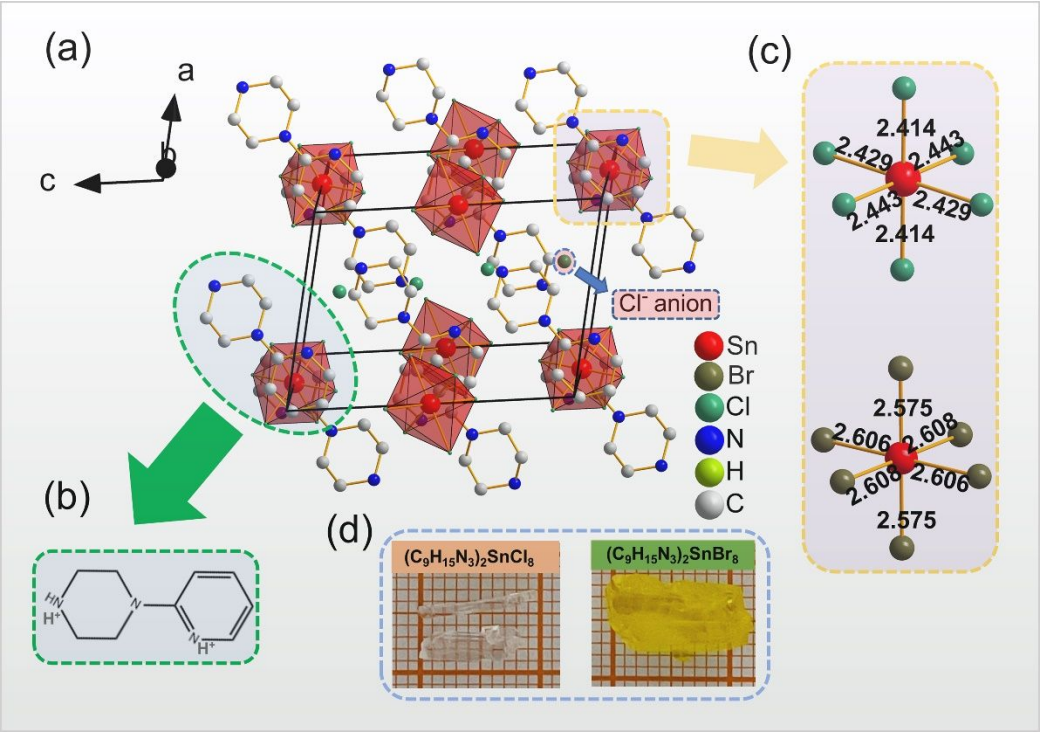

Figure 1. (a) Single-crystal structure of $(C_9H_{15}N_3)_2SnCl_8$ with hydrogen omitted for clarity. (b) Structure of organic cation $(C_9H_{15}N_3)^{2+}$. (c) Two different coordination environments of Sn^{4+}. (d) Photographs of obtained single crystals in sunlight.

$(C_9H_{15}N_3)_2SnCl_8$ and $(C_9H_{15}N_3)_2SnBr_8$ isostructurally crystallize in the monoclinic space group $P2_1/c$. The structural details are provided in **Table 1** and **S1–S8**. The inorganic octahedra composed of Sn cations surrounded by six Cl anions are separated by organic $(C_9H_{15}N_3)^{2+}$ cations, and isolated halogen anions coexist to form the 0D structure. The isolated halogen anions were also reported in other OIMHs.[22, 31] For $(C_9H_{15}N_3)_2SnCl_8$, the bond lengths of Sn–Cl range from 2.4136(4) to 2.4431(4) Å, and the bond angles of Cl–Sn–Cl vary from 87.630(15)° to 92.371(15)°. For $(C_9H_{15}N_3)_2SnBr_8$, the bond length of Sn–Br is longer, ranging from 2.5752

(4) to 2.6078 (4) Å, and the bond angles of Br–Sn–Br range from 87.670(14)° to 92.330(14)°. The distortion of the octahedron of $(C_9H_{15}N_3)_2SnCl_8$ and $(C_9H_{15}N_3)_2SnBr_8$ can be calculated using the following equations:[32]

$$\lambda_{oct} = \frac{1}{6}\sum_{n=1}^{6}[(l_n - l_0)/l_0]^2$$

$$\sigma^2 = \frac{1}{11}\sum_{n=1}^{12}(\theta_n - 90^\circ)^2$$

where d_n is the bond length between Sn and its surrounding six halogen atoms (Cl, Br), d_0 is the average Sn–*X* (*X* = Cl, Br) bond distance, and θ_n is the *X*–Sn–*X* bond angle. The distortion of $(C_9H_{15}N_3)_2SnCl_8$ is only λ_{oct} = 2.38×10^{-5} and σ^2 = 2.52, and similar distortion for $(C_9H_{15}N_3)_2SnBr_8$ of λ_{oct} = 3.38×10^{-5} and σ^2 = 2.22 was observed. The inorganic parts of $(C_9H_{15}N_3)_2SnCl_8$ and $(C_9H_{15}N_3)_2SnBr_8$ form close to normal octahedra, which is similar to the structure of reported Sn^{4+} compounds such as $(C_6N_2H_{16}Cl)_2SnCl_6$[22] and $(C_5H_{14}N_2)_2[SnCl_6]_2\cdot 5H_2O$.[14] Compared with other reported 5s^2-lone-pair-containing Sn^{2+}-based OIMHs, the distortion is much smaller, i.e., $(C_4N_2H_{14}Br)_4SnBr_6$ (λ_{oct} = 4.57×10^{-3}, σ^2 = 18.20) and $(C_4N_2H_{14}Br)_4SnI_6$ (λ_{oct} = 1.57×10^{-3}, σ^2 = 19.45).[23]

Table 1. Crystal data and structure refinement for $(C_9H_{15}N_3)_2SnCl_8$, $(C_9H_{15}N_3)_2SnBr_8$, and $(C_9H_{15}N_3)_2Sn_{0.25}Sb_{0.75}Cl_8$ at 150.0 K.

Empirical formula	$(C_9H_{15}N_3)_2SnCl_8$	$(C_9H_{15}N_3)_2SnBr_8$	$(C_9H_{15}N_3)_2Sn_{0.25}Sb_{0.75}Cl_8$
Formula weight	732.77	544.22	733.53
Temperature	150.0 K	150.0 K	150.0 K
Wavelength	0.71073 Å	0.71073 Å	0.71073 Å
Crystal system	monoclinic	monoclinic	monoclinic
Space group	$P2_1/c$	$P2_1/c$	$P2_1/c$
Unit-cell dimensions	a = 8.9022(2) Å, b = 12.7690(3) Å, c = 12.5449(3) Å, β = 101.299(1)°	a = 9.2518(4) Å, b = 13.1386(6) Å, c = 12.8258(6) Å, β = 101.206(2)°	a = 8.9165(4) Å, b = 12.7460(5) Å, c = 12.5181(5) Å, β = 101.122(2)°
Volume	1398.37(6) Å^3	1529.33(12) Å^3	1395.96(10) Å^3
Z	2	2	2
Density (calculated)	1.740 g/cm^3	2.364 g/cm^3	1.745 g/cm^3
Absorption coefficient	1.699 mm^{-1}	11.306 mm^{-1}	1.720 mm^{-1}
F (000)	732	1020	732
θ range for data collection	2.299° to 26.383°	2.728° to 26.397°	2.824° to 24.997°
Index ranges	$-10 \le h \le 11$, $-15 \le k \le 15$, $-15 \le l \le 15$	$-10 \le h \le 11$, $-15 \le k \le 15$, $-15 \le l \le 15$	$-10 \le h \le 10$, $-15 \le k \le 15$, $-14 \le l \le 14$
Reflections collected	22895	27092	19412
Independent reflections	2865 [R_{int} = 0.0260]	3121 [R_{int} = 0.0713]	2434 [R_{int} = 0.0433]
Completeness to θ = 25.242°	99.9%	99.6%	99%
Refinement method	Full-matrix least-squares on F^2	Full-matrix least-squares on F^2	Full-matrix least-squares on F^2
Data/restraints/parameters	2865/0/151	3121/0/151	2434/0/151
Goodness-of-fit	1.048	1.023	1.140
Final R indices [$I > 2\sigma(I)$]*	R_{obs} = 0.0164, wR_{obs} = 0.0406	R_{obs} = 0.0271, wR_{obs} = 0.0632	R_{obs} = 0.0303, wR_{obs} = 0.0712
R indices [all data]	R_{all} = 0.0190, wR_{all} = 0.0416	R_{all} = 0.0353, wR_{all} = 0.0664	R_{all} = 0.0334, wR_{all} = 0.0730
Largest diff. peak and hole	0.362 and -0.169 e·Å^{-3}	0.683 and -0.469 e·Å^{-3}	0.478 and -0.716 e·Å^{-3}

For $(C_9H_{15}N_3)_2SnCl_8$, $R = \Sigma||F_o|-|F_c||/\Sigma|F_o|$, $wR = \{\Sigma[w(|F_o|^2 - |F_c|^2)^2]/\Sigma[w(|F_o|^4)]\}^{1/2}$ and calc $w = 1/[\sigma^2(F_o^2) + (0.0205P)^2 + 0.4281\mathrm{P}]$, where $P = (F_o^2 + 2F_c^2)/3$;

For $(C_9H_{15}N_3)_2SnBr_8$, $R = \Sigma||F_o|-|F_c||/\Sigma|F_o|$, $wR = \{\Sigma[w(|F_o|^2 - |F_c|^2)^2]/\Sigma[w(|F_o|^4)]\}^{1/2}$ and calc $w = 1/[\sigma^2(F_o^2) + (0.0349P)^2]$, where $P = (F_o^2 + 2F_c^2)/3$;

For $(C_9H_{15}N_3)_2Sn_{0.5}Sb_{0.5}Cl_8$, $R = \Sigma||F_o|-|F_c||/\Sigma|F_o|$, $wR = \{\Sigma[w(|F_o|^2 - |F_c|^2)^2]/\Sigma[w(|F_o|^4)]\}^{1/2}$ and calc $w = 1/[\sigma^2(F_o^2) + (0.0327P)^2 + 1.5196P]$, where $P = (F_o^2 + 2F_c^2)/3$.

The XPS spectra of the two compounds both reveal two peaks near 487.3 and 495.7 eV, which were attributed to the 3*d* orbital of the Sn^{4+} cation, thus verifying the sole existence of the +4 valence state of Sn (**Figure 2**).[22] The band valence sums of the Sn cation in $(C_9H_{15}N_3)_2SnCl_8$ and $(C_9H_{15}N_3)_2SnBr_8$ were calculated to be 3.97 and 3.54, respectively, further verifying the +4 valence state of Sn.

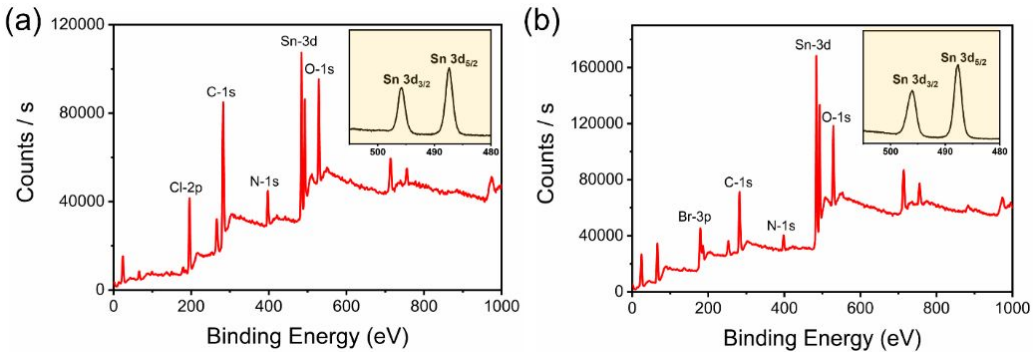

Figure 2. XPS spectra of (a) $(C_9H_{15}N_3)_2SnCl_8$ and (b) $(C_9H_{15}N_3)_2SnBr_8$. The insets show the high-resolution Sn 3*d* peaks.

The experimental and simulated PXRD patterns of both compounds are consistent (**Figure S2**), with no extra peaks observed, indicating that pure phases were obtained. The thermal stabilities of $(C_9H_{15}N_3)_2SnCl_8$ and $(C_9H_{15}N_3)_2SnBr_8$ were explored, with decomposition temperatures of 264 °C and 276 °C, respectively, as shown in (**Figure S3**). $(C_9H_{15}N_3)_2SnCl_8$ and $(C_9H_{15}N_3)_2SnBr_8$ exhibit better thermal stability than Sn^{2+}-based compounds.[4, 23] For $(C_9H_{15}N_3)_2SnCl_8$, a two-step decomposition process is clearly observed. The first decomposition step resulted in a total mass

loss of ~54%, which can be attributed to the volatilization of $C_9H_{14}N_3Cl$; the calculated value is 54.64%. After the second step of decomposition, only 15% of the mass remained. Similarly, $(C_9H_{15}N_3)_2SnBr_8$ underwent a two-step decomposition process, with 44% of its total mass lost in the first decomposition step, which is nearly equivalent to the volatilization of $C_9H_{14}N_3Br$ (the calculated value is 45.04%). After the second decomposition step, almost all of the mass was lost. The thermal stabilities of the two compounds are similar to that of the reported Sn^{4+}-based compound $(C_5N_2H_{14})SnCl_6$, which had a decomposition temperature of 264 °C.[21]

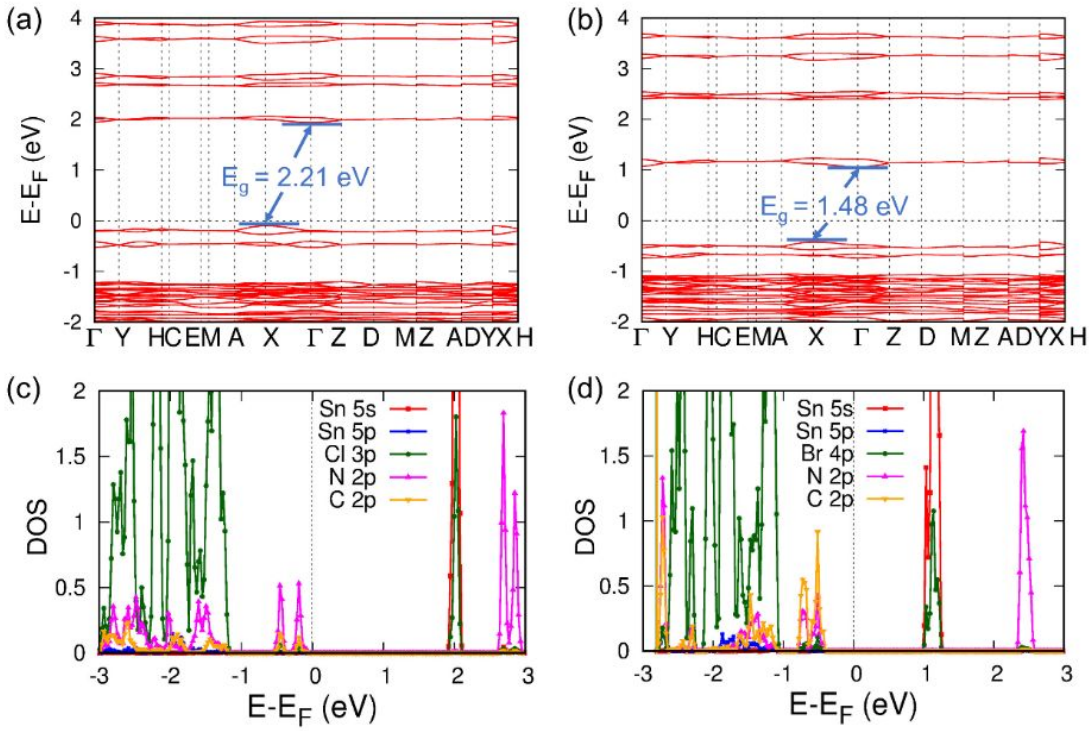

Figure 3. Band structures of (a) $(C_9H_{15}N_3)_2SnCl_8$ and (b) $(C_9H_{15}N_3)_2SnBr_8$. DOS of (c) $(C_9H_{15}N_3)_2SnCl_8$ and d) $(C_9H_{15}N_3)_2SnBr_8$.

The optical band gaps of $(C_9H_{15}N_3)_2SnCl_8$ and $(C_9H_{15}N_3)_2SnBr_8$ were determined from UV–vis diffuse spectra (**Figure S2**). $(C_9H_{15}N_3)_2SnBr_8$ has a relatively small band gap of 2.60 eV, whereas

$(C_9H_{15}N_3)_2SnCl_8$ has a larger one (3.19 eV), which is consistent with the transparent crystal color. The electronic band structure and density of states (DOS) of $(C_9H_{15}N_3)_2SnCl_8$ and $(C_9H_{15}N_3)_2SnBr_8$ were calculated using DFT (**Figure 3)**. For both compounds, the energy band is not very diffuse, indicating the formation of isolated centers. The characteristics of indirect band gaps for both $(C_9H_{15}N_3)_2SnCl_8$ and $(C_9H_{15}N_3)_2SnBr_8$ were determined, with band gaps of 2.21 and 1.48 eV, respectively. Usually, the calculated DFT value underestimates the band gap, which was also the case for the title compounds.[33] For $(C_9H_{15}N_3)_2SnCl_8$, the valence band maximum (VBM) at *X* is composed of N 2p, Cl 3p, and C 2p states, and the conduction band minimum (CBM) at *Γ* is composed of Sn 5s and Cl 3p states. Similarly, the VBM of $(C_9H_{15}N_3)_2SnBr_8$ is mainly composed of N 2p, Br 4p, and C 2p states, and the CBM at *Γ* is composed of Sn 5s and Br 4p states.

The optical properties of $(C_9H_{15}N_3)_2SnCl_8$ and $(C_9H_{15}N_3)_2SnBr_8$ were explored. Under 365-nm excitation, $(C_9H_{15}N_3)_2SnCl_8$ exhibited two emission peaks centered at 405 and 688 nm (**Figure S4**). The best excitation peak monitored at 405 nm was located at 328 nm, with a Stokes shift of 77 nm (0.72 eV). The best excitation peak monitored at 688 nm emission band was located at 378 nm with a Stokes shift of 287 nm (1.48 eV). The PL spectra of the organic raw material $C_9H_{13}N_3$ were collected, and under excitation of 328 and 378 nm, a PL peak centered at 405 nm appeared, which matches well with the high-energy PL peak of $(C_9H_{15}N_3)_2SnCl_8$ (**Figure S5**). The organic ions involved in the PL are also consistent with the calculated band-edge compositions obtained by the DFT calculations. Therefore, the high-energy emission peak is attributed to the organic moiety. This type of organic ion contributing to the PL has been reported in many 0D OIHMs,

including $[(N\text{-}AEPz)ZnCl_4]Cl$ (N-AEPz = N-aminoethylpiperazine),[34] $(TAE)_2[Pb_2Cl_{10}](Cl)_2$ (TAE = tris(2aminoethyl)ammonium),[7] and TPP_2ZnCl_4 (TPP = tetraphenylphosphonium).[35] Similar to other reported compounds, both title Sn^{4+}-based OIMHs exhibited poor luminescent properties.[36] The luminous performance of $(C_9H_{15}N_3)_2SnCl_8$ was poor, with a PLQY of only 1%. For $(C_9H_{15}N_3)_2SnBr_8$, the emission and excitation spectra were too weak to be detected at room temperature.

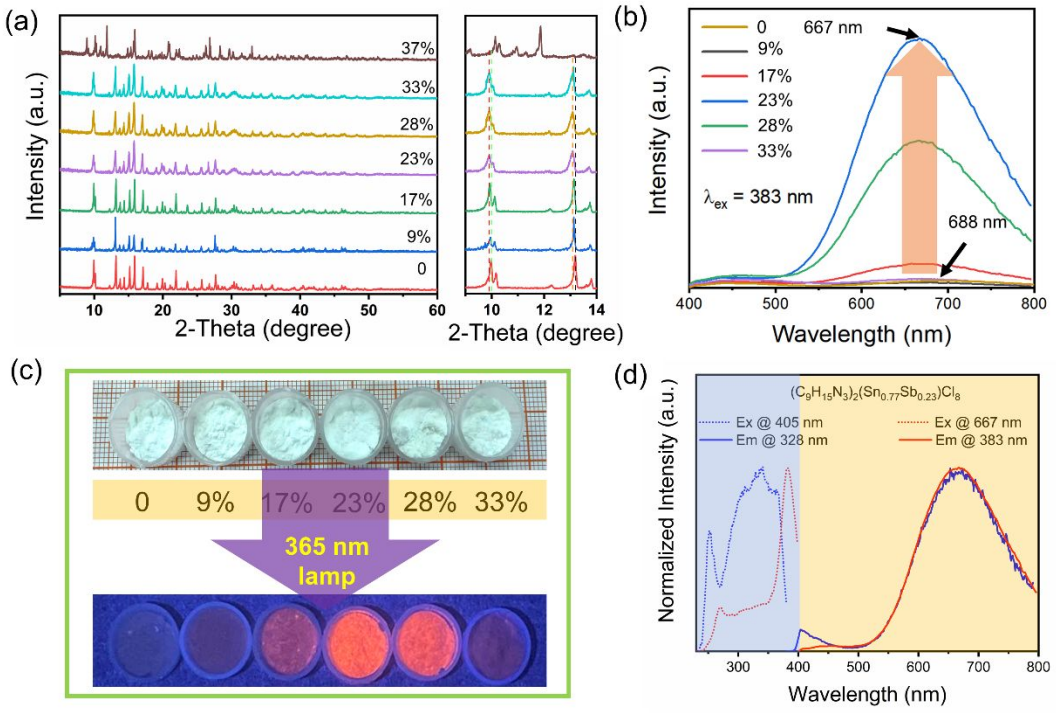

Figure 4. (a) PXRD patterns of Sb^{3+}-doped $(C_9H_{15}N_3)_2SnCl_8$ and selected diffraction peaks in the range of 9°-14°. (b) Emission spectra of $(C_9H_{15}N_3)_2SnCl_8$ powder with different Sb doping contents under 383-nm excitation. (c) Image of Sb^{3+}-doped $(C_9H_{15}N_3)_2SnCl_8$ powder with different Sb doping contents under sunlight and 365-nm lamp. (d) Normalized excitation and emission spectra of $(C_9H_{15}N_3)_2(Sn_{0.77}Sb_{0.23})Cl_8$ powders.

Because the cation radii are very similar (Sb^{3+} can share the same site with Sn^{4+}) and the lone electron pair of Sb^{3+} can enhance the PL of $(C_9H_{15}N_3)_2SnCl_8$,[37, 38] Sb-doped $(C_9H_{15}N_3)_2(Sn_{1-x}Sb_x)Cl_8$ (x = 0.09, 0.17, 0.23, 0.28, 0.33) were synthesized. The PXRD patterns of this series of samples are consistent with that of $(C_9H_{15}N_3)_2SnCl_8$, and no impurity was observed until the doping level reached x = 0.37 (**Figure 4a**). Diffraction peaks are shifted to lower angles due to larger lattice parameters as the doping level increases, in accordance with fact atomic radii size (**Figure 4a**). The relevant EDS analysis data of Sb^{3+}-doped $(C_9H_{15}N_3)_2SnCl_8$ is shown in **Figure S6**. EDS elemental analysis proved that Sb/Sn increased linearly with increasing feed ratio (**Figure S7a)**. Elemental mapping of the $(C_9H_{15}N_3)_2(Sn_{0.77}Sb_{0.23})Cl_8$ sample confirmed the successful doping of the Sb element, and further ICP-OES measurements gave a Sb/Sn ratio of 0.22 (**Figure S7b**). Under 383-nm excitation, $(C_9H_{15}N_3)_2(Sn_{0.77}Sb_{0.23})Cl_8$ exhibited the most intense PL (**Figure 4b**) and also showed the strongest absorption, as given by the absorption spectra of different doping levels (**Figure S7c**). **Figure S8** shows the CIE color coordinate change of Sb^{3+}-doped $(C_9H_{15}N_3)_2SnCl_8$. Under 365-nm light (**Figure 4c**), the samples with different doping levels exhibited clearly different luminescence intensities. Similar to the undoped sample, two emission peaks were observed for all the doping levels (**Figure 4d**). Through Sb doping, the PLQY of $(C_9H_{15}N_3)_2SnCl_8$ is significantly increased from ~1% to 17.84%. To investigate the stability of the samples before and after doping, the PXRD patterns after storage in air for three months were consistent with those of the fresh samples, indicating that both $(C_9H_{15}N_3)_2SnCl_8$ and

$(C_9H_{15}N_3)_2(Sn_{0.77}Sb_{0.23})Cl_8$ had good air stability. $(C_9H_{15}N_3)_2(Sn_{0.77}Sb_{0.23})Cl_8$ is stable at 262 ℃ (**Figure S9**).

In $(C_9H_{15}N_3)_2SnCl_8$, Sn (IV) ($4d^{10}5s^0$) lacks stereochemical-activity outermost electrons, and the material exhibits poor luminescence. After doping, due to the highly active $5s^2$ lone pair of Sb(III), the probability of electron transition to the excitation state was enhanced, resulting in more effective emission.[28] Alternatively, from the perspective of the widely accepted STE emission, which can be alternatively expressed as ns^2 emission in lone-pair-containing isolated cations, the octahedral distortion plays a crucial role in the formation of self-trapped excitons.[39-41] The structure of $(C_9H_{15}N_3)_2(Sn_{0.77}Sb_{0.23})Cl_8$, with a nominal formula of $(C_9H_{15}N_3)_2(Sn_{0.75}Sb_{0.25})Cl_8$ from single-crystal diffraction (Table 1), exhibited greater distortion ($\lambda_{oct} = 7.64\times10^{-5}$ and $\sigma^2 = 3.06$) than the undoped sample (**Figure S10**). This result indicates that Sb^{3+} doping can be used as an effective way to enhance the emission intensity of Sn^{4+}-based compounds.

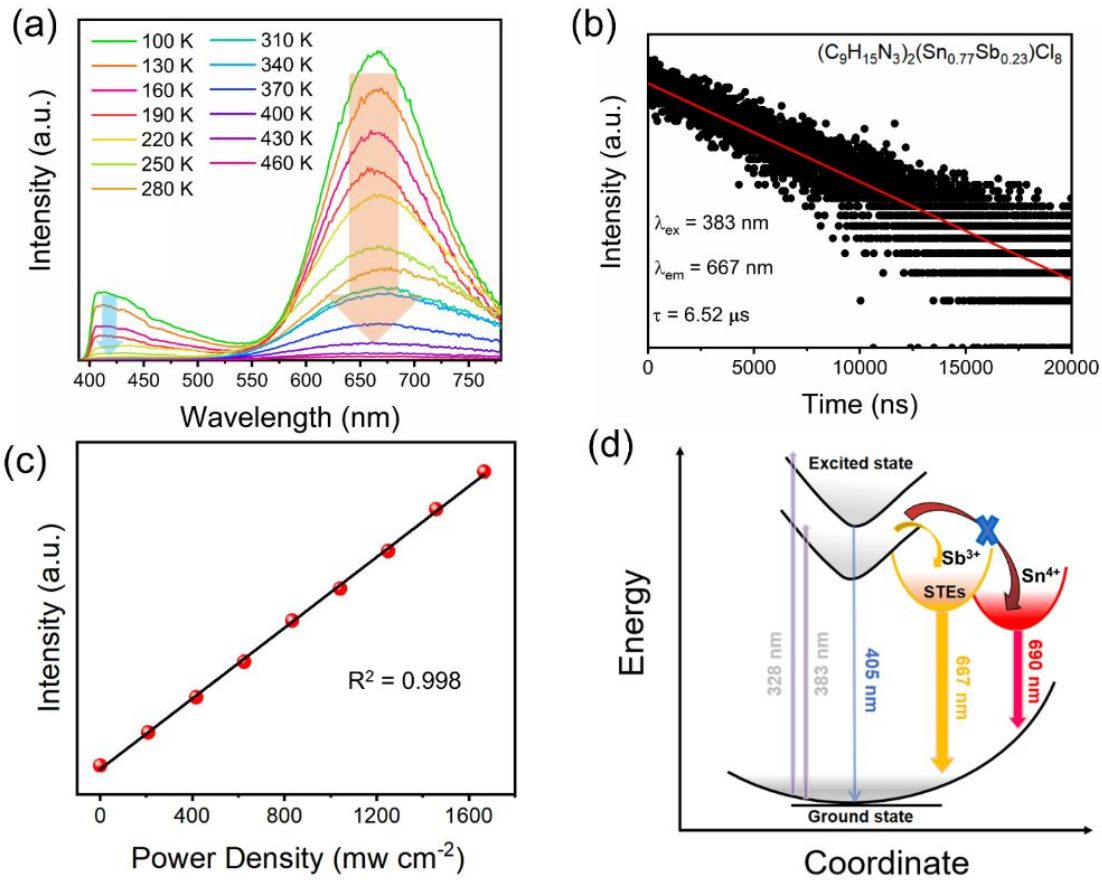

Figure 5. a) Temperature dependence of PL spectra of $(C_9H_{15}N_3)_2(Sn_{0.77}Sb_{0.23})Cl_8$. b) PL decay curves of $(C_9H_{15}N_3)_2(Sn_{0.77}Sb_{0.23})Cl_8$ at 100 K. c) Emission intensity versus excitation power for $(C_9H_{15}N_3)_2(Sn_{0.77}Sb_{0.23})Cl_8$. d) Configuration coordinate diagram of $(C_9H_{15}N_3)_2(Sn_{0.77}Sb_{0.23})Cl_8$.

To better understand the emission mechanism, low-temperature spectra of both $(C_9H_{15}N_3)_2SnCl_8$ and $(C_9H_{15}N_3)_2(Sn_{0.77}Sb_{0.23})Cl_8$ were collected. With decreasing temperature, the emission intensity of both compounds monotonously increased due to the non-radiative process decreasing (**Figure 5a**). From the normalized PL peaks of $(C_9H_{15}N_3)_2(Sn_{0.77}Sb_{0.23})Cl_8$, it is obvious that the positions of the low-energy emission peak (667 nm) remain unchanged with increasing temperature, and the broadening is due to the increased thermal vibrational dynamics at higher temperatures

(**Figure S11**). These results indicate that the emission mechanism of the low-energy peak is more in line with STE emission.[42] The long decay lifetime at 100 K (6.52 μs) also confirmed this finding (**Figure 5b**).[21, 24] With decreasing temperature (**Figure S11b**), the emission peak position of $(C_9H_{15}N_3)_2SnCl_8$ moved from 675 (100 K) to 688 nm (320 K), which is due to the bandgap decrease resulting from the increased temperature, a very common phenomenon in semiconductors. Unlike in the undoped sample, the low-energy emission peak of $(C_9H_{15}N_3)_2(Sn_{0.77}Sb_{0.23})Cl_8$ did not change significantly at 667 nm, indicating more stable optical properties. The PL spectra of $(C_9H_{15}N_3)_2(Sn_{0.77}Sb_{0.23})Cl_8$ were collected with different excitation power levels (**Figure 5c**), with the excitation energy increasing linearly with no saturation observed, indicating that the broadband emission does not originate from permanent defects. Therefore, it is further proved that the low-energy peak originates from the ns^2 emission of lone-pair-containing Sb^{3+}. This photophysical process (**Figure 5d**) can be described as follows: under the excitation of higher energy (328 nm), the electron will be promoted to a higher excited state and then returned to the ground state by radiation, resulting in an emission in the range of 380–550 nm. For undoped parent, Sn^{4+} ($5s^0$) lacks a stereochemical active lone pair and exhibits poor luminescent performance. After Sb^{3+} doping, because Sb^{3+} has a highly active $5s^2$ lone pair, the probability of exciton self-trapping to form the STE emission of Sb^{3+} increases, peaking at 667 nm.

Conclusion

Two novel OIMHs $(C_9H_{15}N_3)_2SnX_8$ (X = Cl, Br) with 0D structure were synthesized using environmentally friendly Sn^{4+} as the metal cation. The decomposition temperatures of the two

compounds were above 260 °C, indicating remarkable stability. $(C_9H_{15}N_3)_2SnCl_8$ exhibited double-peak emission at 405 and 688 nm, which was attributed to emission from organic cations and inorganic octahedra, respectively. After the introduction of Sb cations with active $5s^2$ lone-pair electrons in $(C_9H_{15}N_3)_2SnCl_8$, the PLQY greatly increased, form 1% to 17.84%. The highly efficient emission of the Sb-doped $(C_9H_{15}N_3)_2SnCl_8$ samples is attributed to the enhanced distortion of the inorganic octahedra caused by ns^2 electrons resulting in promoted STE emission. This work provides a new route for the design of more stable and environmentally friendly luminescent materials and paves the way for optimizing the optical properties via doping with lone-pair containing cations.

Associated content

Electronic supplementary information (ESI) available: Tables of atomic coordinates, displacement parameters, anisotropic displacement parameters, and bond distances of $(C_9H_{15}N_3)_2SnCl_8$ and $(C_9H_{15}N_3)_2SnBr_8$; EDS, SEM, X-ray diffraction pattern, band gap, TGA of $(C_9H_{15}N_3)_2SnCl_8$ and $(C_9H_{15}N_3)_2SnBr_8$; temperature-dependent steady-state PL spectra, excitation and emission spectra, PL decay curves, configuration coordinate diagram of $(C_9H_{15}N_3)_2SnCl_8$; normalized emission spectra of organic molecular and $(C_9H_{15}N_3)_2SnCl_{8;}$ elemental mapping, crystal structure of $(C_9H_{15}N_3)_2(Sn_{0.75}Sb_{0.25})Cl_{8;}$ absorption spectra of $(C_9H_{15}N_3)_2SnCl_8$ with different doping levels. See DOI:

CCDC 2156933-2156935 contains supplementary crystallographic data for this study.

Corresponding author

* jingzhao@ustb.edu.cn

Conflicts and interest

The authors declare no competing financial interest.

Acknowledgements

This study was supported by The National Key Research and Development Program of China (2021YFA0718900), the National Natural Science Foundation of China (51972021), and the Fundamental Research Funds for the Central Universities FRF-IDRY-19-005. SH and CW are supported by the U.S Department of Energy, Office of Science and Office of Basic Energy Sciences under award number DE-SC0014520.

Notes and references

1 Q. Zhang, S. T. Ha, X. Liu, T. C. Sum, Q. Xiong, Room-Temperature Near-Infrared High-Q Perovskite Whispering-Gallery Planar Nanolasers, *Nano Lett.,* **2014,** *14* (10), 5995-6001.

2 Z. Song, J. Zhao, Q. Liu, Luminescent Perovskites: Recent Advances in Theory and Experiments, *Inorg. Chem. Front.,* **2019,** *6* (11), 2969-3011.

3 J. Xu, X. Li, J. Xiong, C. Yuan, S. Semin, T. Rasing, X. H. Bu, Halide Perovskites for Nonlinear Optics, *Adv. Mater.,* **2020,** *32* (3), 1806736.

4 C. Zhou, H. Lin, H. Shi, Y. Tian, C. Pak, M. Shatruk, Y. Zhou, P. Djurovich, M.-H. Du, B. Ma, A Zero-Dimensional Organic Seesaw-Shaped Tin Bromide with Highly Efficient Strongly Stokes-Shifted Deep-Red Emission, *Angew. Chem. Int. Ed.,* **2018,** *57* (4), 1021-1024.

5 C. Zhou, H. Lin, H. Shi, Y. Tian, C. Pak, M. Shatruk, Y. Zhou, P. Djurovich, M. H. Du,

B. Ma, A Zero-Dimensional Organic Seesaw-Shaped Tin Bromide with Highly Efficient Strongly Stokes-Shifted Deep-Red Emission, *Angew. Chem. Int. Ed.,* **2018,** *57* (4), 1021-1024.

6 H. Lin, C. Zhou, Y. Tian, T. Siegrist, B. Ma, Low-Dimensional Organometal Halide Perovskites, *ACS Energy Lett.,* **2018,** *3* (1), 54.

7 S. Elleuch, A. Lusson, S. Pillet, K. Boukheddaden, Y. Abid, White Light Emission from a Zero-Dimensional Lead Chloride Hybrid Material, *ACS Photonics,* **2020,** *7* (5), 1178-1187.

8 C. Deng, G. Zhou, D. Chen, J. Zhao, Y. Wang, Q. Liu, Broadband Photoluminescence in 2D Organic–Inorganic Hybrid Perovskites: $(C_7H_{18}N_2)PbBr_4$ and $(C_9H_{22}N_2)PbBr_4$, *J. Phys. Chem. Lett.,* **2020,** *11* (8), 2934-2940.

9 J. E. Thomaz, K. P. Lindquist, H. I. Karunadasa, M. D. Fayer, Single Ensemble Non-exponential Photoluminescent Population Decays from a Broadband White-Light-Emitting Perovskite, *J. Am. Chem. Soc.,* **2020,** *142* (39), 16622-16631.

10 I. Neogi, A. Bruno, D. Bahulayan, T. W. Goh, B. Ghosh, R. Ganguly, D. Cortecchia, T. C. Sum, C. Soci, N. Mathews, S. G. Mhaisalkar, Broadband-Emitting 2 D Hybrid Organic–Inorganic Perovskite Based on Cyclohexane-bis(methylamonium) Cation, *ChemSusChem,* **2017,** *10* (19), 3765-3772.

11 K. Tao, Y. Li, C. Ji, X. Liu, Z. Wu, S. Han, Z. Sun, J. Luo, A Lead-Free Hybrid Iodide with Quantitative Response to X-ray Radiation, *Chem. Mater.,* **2019,** *31* (15), 5927-5932.

12 S. Sun, S. Tominaka, J. H. Lee, F. Xie, P. D. Bristowe, A. K. Cheetham, Synthesis, Crystal Structure and Properties of a Perovskite-Related Bismuth Phase, $(NH_4)_3Bi_2I_9$, *APL Mater.,* **2015,** *4* (3), 6050-6051.

13 I. Feddaoui, M. S. M. Abdelbaky, S. García-Granda, K. Essalah, C. Ben Nasr, M. L. Mrad, Synthesis, Crystal Structure, Vibrational Spectroscopy, DFT, Optical Study and Thermal Analysis of a New Stannate(IV) Complex Based on 2-ethyl-6-methylanilinium $(C_9H_{14}N)_2[SnCl_6]$, *J. Mol.*

Struct., **2019,** *1186*, 31-38.

14 S. BelhajSalah, M. S. M. Abdelbaky, S. García-Granda, K. Essalah, C. Ben Nasr, M. L. Mrad, Synthesis, Crystal Structure, Vibrational, Optical Properties, Thermal Analysis and Theoretical Study of a New Sn(IV) Complex $(C_5H_{14}N_2)_2[SnCl_6]_2 \cdot 5H_2O$, *Solid State Sci.,* **2018,** *86*, 77-85.

15 Y. Jing, Y. Liu, J. Zhao, Z. Xia, Sb^{3+} Doping-Induced Triplet Self-Trapped Excitons Emission in Lead-Free Cs_2SnCl_6 Nanocrystals, *J. Phys. Chem. Lett.,* **2019,** *10* (23), 7439-7444.

16 A. E. Maughan, A. M. Ganose, D. O. Scanlon, J. R. Neilson, Perspectives and Design Principles of Vacancy-Ordered Double Perovskite Halide Semiconductors, *Chem. Mater.,* **2019,** *31* (4), 1184-1195.

17 Z. Tan, J. Li, C. Zhang, Z. Li, Q. Hu, Z. Xiao, T. Kamiya, H. Hosono, G. Niu, E. Lifshitz, Y. Cheng, J. Tang, Highly Efficient Blue-Emitting Bi-Doped Cs_2SnCl_6 Perovskite Variant: Photoluminescence Induced by Impurity Doping, *Adv. Funct. Mater.,* **2018,** *28* (29), 1801131.

18 L. Zhou, J. Liao, Z. Huang, J. Wei, X. Wang, H. Chen, D. Kuang, Intrinsic Self-Trapped Emission in 0D Lead-Free $(C_4H_{14}N_2)_2In_2Br_{10}$ Single Crystal, *Angew. Chem.,* **2019,** *131* (43), 15581-15586.

19 B. Lee, C. C. Stoumpos, N. Zhou, F. Hao, C. Malliakas, C.-Y. Yeh, T. J. Marks, M. G. Kanatzidis, R. P. H. Chang, Air-Stable Molecular Semiconducting Iodosalts for Solar Cell Applications: Cs_2SnI_6 as a Hole Conductor, *J. Am. Chem. Soc.,* **2014,** *136* (43), 15379-15385.

20 T. Dammak, Y. Abid, Quasi-White Light Emission Involving Förster Resonance Energy Transfer In a New Organic Inorganic Tin Chloride Based Material (AMPS)$[SnCl_6]H_2O$, *Opt. Mater.,* **2017,** *66*, 302-307.

21 G. Song, Z. Li, P. Gong, R.-J. Xie, Z. Lin, Tunable White Light Emission in a Zero-Dimensional Organic–Inorganic Metal Halide Hybrid with Ultra-High Color Rendering Index, *Adv.*

Optical Mater. , **2021,** *9* (11), 2002246.

22 G. Song, M. Li, Y. Yang, F. Liang, Q. Huang, X. Liu, P. Gong, Z. Xia, Z. Lin, Lead-Free Tin(IV)-Based Organic–Inorganic Metal Halide Hybrids with Excellent Stability and Blue-Broadband Emission, *J. Phys. Chem. Lett.,* **2020,** *11* (5), 1808-1813.

23 C. Zhou, H. Lin, Y. Tian, Z. Yuan, R. Clark, B. Chen, L. J. van de Burgt, J. C. Wang, Y. Zhou, K. Hanson, Q. J. Meisner, J. Neu, T. Besara, T. Siegrist, E. Lambers, P. Djurovich, B. Ma, Luminescent Zero-Dimensional Organic Metal Halide Hybrids with Near-Unity Quantum Efficiency, *Chem. Sci.,* **2018,** *9* (3), 586-593.

24 M. Li, Z. Xia, Recent Progress of Zero-Dimensional Luminescent Metal Halides, *Chem. Soc. Rev.,* **2021,** *50* (4), 2626-2662.

25 P. Boutinaud, Luminescence of Sb^{3+} in Closed Shell Transition Metal Oxides, *J. Lumin.,* **2019,** *208*, 394.

26 H. Arfin, A. S. Kshirsagar, J. Kaur, B. Mondal, Z. Xia, S. Chakraborty, A. Nag, ns^2 Electron (Bi^{3+} and Sb^{3+}) Doping in Lead-Free Metal Halide Perovskite Derivatives, *Chem. Mater.,* **2020,** *32*, 10255.

27 G. Zhang, P. Dang, H. Xiao, H. Lian, S. Liang, L. Yang, Z. Cheng, G. Li, J. Lin, Antimony-Doped Lead-Free Zero-Dimensional Tin(IV)-Based Organic–Inorganic Metal Halide Hybrids with High Photoluminescence Quantum Yield and Remarkable Stability, *Adv. Optical Mater.,* **2021,** *9* (24), 2101637.

28 L. Zhou, L. Zhang, H. Li, W. Shen, M. Li, R. He, Defect Passivation in Air-Stable Tin(IV)-Halide Single Crystal for Emissive Self-Trapped Excitons, *Adv. Funct. Mater.,* **2021,** *31* (51), 2108561.

29 G. M. Sheldrick, A Short History of SHELX, *Acta Crystallogr.,Sect. A: Found. Crystallogr.,* **2008,** *64*, 112-122.

30 G. Kresse, J. Furthmüller, Efficient iterative schemes for AB Initio Total-Energy Calculations Using a Plane-Wave Basis Set, *Phys. Rev. B: Condens. Matter Mater. Phys.,* **1996,** *54* (16), 11169-11186.

31 D. Chen, S. Hao, L. Fan, Y. Guo, J. Yao, C. Wolverton, M. G. Kanatzidis, J. Zhao, Q. Liu, Broad Photoluminescence and Second-Harmonic Generation in the Noncentrosymmetric Organic–Inorganic Hybrid Halide $(C_6H_5(CH_2)_4NH_3)_4MX_7{\cdot}H_2O$ (M = Bi, In, X = Br or I), *Chem. Mater.,* **2021,** *33* (20), 8106-8111.

32 K. Robinson, G. V. Gibbs, P. H. Ribbe, Quadratic Elongation: A Quantitative Measure of Distortion in Coordination Polyhedra, *Science,* **1971,** *172* (3983), 567.

33 D. Chen, S. Hao, G. Zhou, C. Deng, Q. Liu, S. Ma, C. Wolverton, J. Zhao, Z. Xia, Lead-Free Broadband Orange-Emitting Zero-Dimensional Hybrid $(PMA)_3InBr_6$ with Direct Band Gap, *Inorg. Chem.,* **2019,** *58* (22), 15602-15609.

34 X. Zhang, L. Li, S. Wang, X. Liu, Y. Yao, Y. Peng, M. Hong, J. Luo, $[(N\text{-}AEPz)ZnCl_4]Cl$: A "Green" Metal Halide Showing Highly Efficient Bluish-White-Light Emission, *Inorg. Chem.,* **2020,** *59* (6), 3527-3531.

35 L.-J. Xu, A. Plaviak, X. Lin, M. Worku, Q. He, M. Chaaban, B. J. Kim, B. Ma, Metal Halide Regulated Photophysical Tuning of Zero-Dimensional Organic Metal Halide Hybrids: From Efficient Phosphorescence to Ultralong Afterglow, *Angew. Chem. Int. Ed.,* **2020,** *59* (51), 23067-23071.

36 T. Dammak, Y. Abid, Quasi-White Light Emission Involving Förster Resonance Energy Transfer In a New Organic Inorganic Tin Chloride Based Material $(AMPS)[SnCl_6]H_2O$, *Opt. Mater.,* **2017,** *66*, 302-307.

37 H. Arfin, A. Nag, Origin of Luminescence in Sb^{3+}- and Bi^{3+}-Doped Cs_2SnCl_6 Perovskites: Excited State Relaxation and Spin–Orbit Coupling, *J. Phys. Chem. Lett.,* **2021,** *12* (41), 10002-

10008.

38 B. Zhou, Z. Liu, S. Fang, H. Zhong, B. Tian, Y. Wang, H. Li, H. Hu, Y. Shi, Efficient White Photoluminescence from Self-Trapped Excitons in Sb^{3+}/Bi^{3+}-Codoped $Cs_2NaInCl_6$ Double Perovskites with Tunable Dual-Emission, *ACS Energy Lett.,* **2021,** *6* (9), 3343-3351.

39 M. D. Smith, A. Jaffe, E. R. Dohner, A. M. Lindenberg, H. I. Karunadasa, Structural Origins of Broadband Emission from Layered Pb–Br Hybrid Perovskites, *Chem. Sci.,* **2017,** *8* (6), 4497-4504.

40 L. Mao, Y. Wu, C. C. Stoumpos, B. Traore, C. Katan, J. Even, M. R. Wasielewski, M. G. Kanatzidis, Tunable White-Light Emission in Single-Cation-Templated Three-Layered 2D Perovskites $(CH_3CH_2NH_3)_4Pb_3Br_{10-x}Cl_x$, *J. Am. Chem. Soc.,* **2017,** *139* (34), 11956-11963.

41 L. Mao, Y. Wu, C. C. Stoumpos, M. R. Wasielewski, M. G. Kanatzidis, White-Light Emission and Structural Distortion in New Corrugated Two-Dimensional Lead Bromide Perovskites, *J. Am. Chem. Soc.,* **2017,** *139* (14), 5210-5215.

42 M. S. Molokeev, B. Su, A. S. Aleksandrovsky, N. N. Golovnev, M. E. Plyaskin, Z. Xia, Machine Learning Analysis and Discovery of Zero-Dimensional ns^2 Metal Halides toward Enhanced Photoluminescence Quantum Yield, *Chem. Mater.,* **2022,** *34* (2), 537-546.